Chinese Journal of
POLYMER SCIENCE

RESEARCH ARTICLE

https://doi.org/10.1007/s10118-026-3842-z
Chinese J. Polym. Sci.

Synergistic Hierarchical Hydrogen Bonding and Hydrophobic Association Enable Mechanically Robust Underwater Adhesive Ionogels for Wearable Sensing

Lan Lei*, Xiao-Xuan Liu, Wen-Jie Yang, Yu Xie, Xian-Wen Hong, Yu-Heng Liu, Chun-Jie Xie, Chuan-Yong Zong, and Hui Li*

Shandong Provincial Key Laboratory of Extreme Environment-tolerant Specialty Chemicals, School of Chemistry and Chemical Engineering, University of Jinan, Jinan 250022, China

Electronic Supplementary Information

Abstract The development of underwater adhesive ionogels is severely hindered by the trade-off among mechanical robustness, interfacial adhesion, and interfacial hydration. Herein, we propose a supramolecular design strategy exploiting synergistic hierarchical hydrogen bonding and hydrophobic association to fabricate mechanically robust underwater adhesive ionogels (ITD). Specifically, the ITD is engineered *via* the UV-initiated copolymerization of trifluoroethyl acrylate (TFEA) and diethylacrylamide (DEEA) monomers dissolved in an amphiphilic urea-functionalized fluorinated ionic liquid. Driven by the multiple supramolecular interactions, the resulting ionogel exhibits an exceptional tensile strength of 1.89 MPa alongside a remarkable instantaneous adhesion strength of up to 9.44 MPa. Additionally, it maintains over 90% of its initial mechanical strength and lap-shear strength following an 8-day immersion in water, and exhibits an adhesive strength of 5.33 MPa after a 7-day immersion in simulated seawater, confirming its exceptional interfacial water-repelling capability and long-term underwater stability. Density functional theory (DFT) calculations validated the mechanism underlying the enhancement of underwater cohesion and adhesion. Moreover, the inherently reversible dynamic network endows the ionogel with significant self-healing and welding capabilities, as well as recyclability, achieving efficiencies greater than 85%. The ITD ionogel enables the real-time, high-fidelity monitoring of human electrophysiological signals. This work not only provides a versatile paradigm for designing resilient underwater adhesives, but also highlights their tremendous promise for next-generation wearable healthcare electronics and complex-environment human-machine interfaces.

Keywords Hierarchical hydrogen bonding; Hydrophobic association; High strength; Underwater ionogel adhesive; Flexible wearable sensor

Citation: Lei, L.; Liu, X. X.; Yang, W. J.; Xie, Y.; Hong, X. W.; Liu, Y. H.; Xie, C. J.; Zong, C. Y.; Li, H. Synergistic hierarchical hydrogen bonding and hydrophobic association enable mechanically robust underwater adhesive ionogels for wearable sensing. *Chinese J. Polym. Sci.* https://doi.org/10.1007/s10118-026-3842-z

INTRODUCTION

Driven by rapid paradigm shifts in flexible wearable electronics, next-generation human-machine interfaces, and advanced marine engineering, there is an unprecedented demand for soft conductive adhesives that integrate exceptional mechanical robustness, extreme environmental resilience, and multifunctionality.[1–3] Ionogels, defined as non-volatile ionic liquids (ILs) immobilized within polymeric scaffolds, have emerged as a prominent class of soft materials. Their intrinsic properties, including negligible vapor pressure, superior thermal stability, broad electrochemical windows, and high ionic conductivity, have positioned them at the forefront of modern soft ionotronics.[4–6] However, for practical applications requiring robust interfacial binding, conventional adhesive ionogels in aquatic environments are fundamentally hindered by the irreconcilable trade-off between durable underwater interfacial adhesion and bulk cohesion.[7,8] Upon exposure to water, a dense hydration layer forms at the adhesive-substrate interface, severely limiting non-covalent interactions and effectively obliterating binding sites.[9] Simultaneously, water molecules infiltrate and disrupt the delicate equilibrium of the endogenous physical cross-linking networks within the polymer matrix. Solvent-induced plasticization inevitably leads to substantial volumetric swelling, network disintegration, and catastrophic mechanical failure.[10,11] Consequently, rationally decoupling the complex interplay among the molecular cohesive energy, interfacial adhesion energy, and hydration-induced shielding remains a formidable scientific challenge in the development of next-generation underwater adhesive ionogels.

To address these significant challenges, contemporary re-

* Corresponding authors, E-mail: chm_leil@ujn.edu.cn (L.L.)
E-mail: chm_lih1@ujn.edu.cn (H.L.)
Received July 7, 2026; Accepted August 11, 2026; Published online November 23, 2026

© Chinese Chemical Society
Institute of Chemistry, Chinese Academy of Sciences

search has focused on engineering interfacial water-repelling strategies to enhance underwater adhesion and cohesion of ionogels.[12,13] Research indicates that utilizing oxidative crosslinking and metal coordination of catechol moieties can effectively eliminate interfacial water, thereby promoting robust adhesion.[14,15] However, such rigorous cross-linking typically results in a substantial decrease in the intrinsic mechanical robustness of the ionogels. Furthermore, their inherent pH dependency restricts their broad applicability in non-alkaline aquatic environments.[16,17] An alternative approach involves the incorporation of hydrophobic alkyl or aromatic groups that exploit hydrophobic interactions to direct the topological rearrangement of interfacial polymer chains, thereby creating a hydrophobic barrier that repels water infiltration.[18–21] Nevertheless, the interfacial water-repelling efficiency achieved by relying solely on these weak hydrophobic interactions is inherently limited, rendering it insufficient to mitigate the negative effects of hydration.[22,23] Recent investigations have focused on the fabrication of amphiphilic ionogels by copolymerizing hydrophilic monomers with their fluorine-containing hydrophobic counterparts. This approach aims to synergistically enhance interfacial adhesion energy, molecular cohesion energy, and interfacial water drainage through hydrogen bonding and hydrophobic interactions.[20,24,25] However, their underwater adhesive durability remains critically compromised, failing to meet the stringent demands of practical application in extreme environments.

Our previous investigations have elucidated that bidentate hydrogen bonds originating from high-binding-energy urea motifs can effectively orchestrate the dynamic dissociation and reconstruction of the cross-linked network.[26] This topological evolution dynamically activates the interfacial release of abundant low-binding-energy hydrogen-bonding moieties, thereby securing robust underwater adhesion. Nevertheless, the incorporation of a strongly hydrophilic acrylic network impaired the long-term durability of these ionogels in complex aqueous environments to some extent. Therefore, there is an urgent need to develop a synergistic structural paradigm: constructing a hydrophobic polymer backbone to energetically repel free water and preserve the integrity of bulk cohesion while simultaneously employing an amphiphilic IL as a localized water-binding agent to securely trap residual interfacial moisture, thereby ensuring long-term underwater adhesive durability.

Herein, we propose a supramolecular design strategy exploiting synergistic hierarchical hydrogen bonding and hydrophobic associations to fabricate a mechanically robust and highly durable underwater adhesive ionogel (ITD). The ITD ionogel was synthesized *via in situ* copolymerization of trifluoroethyl acrylate (TFEA) and diethylacrylamide (DEEA) monomers within a structurally tailored, amphiphilic urea-functionalized fluorinated IL. Through rational structural design, the fluorinated TFEA and diethyl groups of DEEA form a critical hydrophobic barrier that effectively repels bulk water, whereas the custom IL serves a significant dual function. Its strong bidentate urea motifs establish highly stable internal cohesive hubs, and its amphiphilic nature acts as a water-binding agent that energetically sequesters the infiltrating interfacial water. The optimal ITD ionogel exhibited an exceptional tensile strength of 1.89 MPa and a remarkable instantaneous adhesion strength of 9.44 MPa. Furthermore, it demonstrates remarkable tolerance to extreme environments, retaining over 90% of its mechanical and adhesive properties after an 8-day immersion in water, which facilitates the decoupling of bulk cohesion and underwater adhesion. Additionally, the dynamic reversibility of the supramolecular network provided ionogels with efficient self-healing, self-welding, and ethanol-assisted recyclability. We further highlight the immense potential of the ITD ionogel as a flexible epidermal electrode for the high-fidelity, real-time monitoring of human electrophysiological signals (ECG and EMG), establishing a versatile paradigm for next-generation wearable healthcare electronics in complex environments.

EXPERIMENTAL

All reagents, detailed synthesis methods, and measurements are listed in the electronic supplementary information (ESI).

RESULTS AND DISCUSSION

Preparation and Internal Interactions of Adhesive Ionogels

As illustrated in Fig. 1(a), the fabrication of the ionogel adhesive commenced with the homogeneous mixing of trifluoroethyl acrylate (TFEA), diethylacrylamide (DEEA), and [BIPIMI][TFSI] ionic liquid (IL), accompanied by the addition of the photoinitiator 184 (1 mol% relative to the total molar number of monomers). The resulting precursor solution was subsequently cast into a silicone mold and subjected to 365 nm ultraviolet (UV) irradiation (power: 200 mW·cm^{-2}) for 1 h to synthesize the ionogel adhesive. To systematically elucidate the underlying structure-property relationship, a series of ionogels with varying monomer and IL contents were prepared. For clarity of presentation, the resulting ionogels are designated as $I_aT_xD_y$. Herein, I, T, and D denote IL, TFEA, and DEEA, respectively. The subscript a indicates the mass fraction of the IL within the overall ionogel, whereas the ratio *x*:*y* represents the specific mass ratio of TFEA to DEEA.

Specific intermolecular interactions, including urea-ester, urea-amide, monodentate, and bidentate hierarchical hydrogen bonds, hydrophobic associations, and ion-dipole interactions, are illustrated in Fig. 1(a). We further examined these interactions using density functional theory (DFT) calculations with the DMol3 module of Materials Studio. As shown in Figs. 1(b) and 1(c) and Table S1 (in ESI), the T-D pair exhibits a modest interaction energy of −1.47 kcal·mol^{-1}. The electrostatic potential (ESP) map of this pair revealed relatively weak electrostatic complementarity, corroborating that their interaction is predominantly governed by weak hydrophobic and dipole-dipole interactions. Notably, the I-T-D pair demonstrated a significantly enhanced interaction energy of −10.86 kcal·mol^{-1}. In the corresponding ESP topography, the strongly positive (red) potential regions localized on the urea protons and imidazolium ring of the IL perfectly complement the strongly negative (blue) potential regions of the carbonyl oxygens and fluorine atoms in TFEA and DEEA. This distinct electrostatic complementarity visually confirms the formation of robust hierarchical hydrogen bonds and ion-dipole in-

https://doi.org/10.1007/s10118-026-3842-z

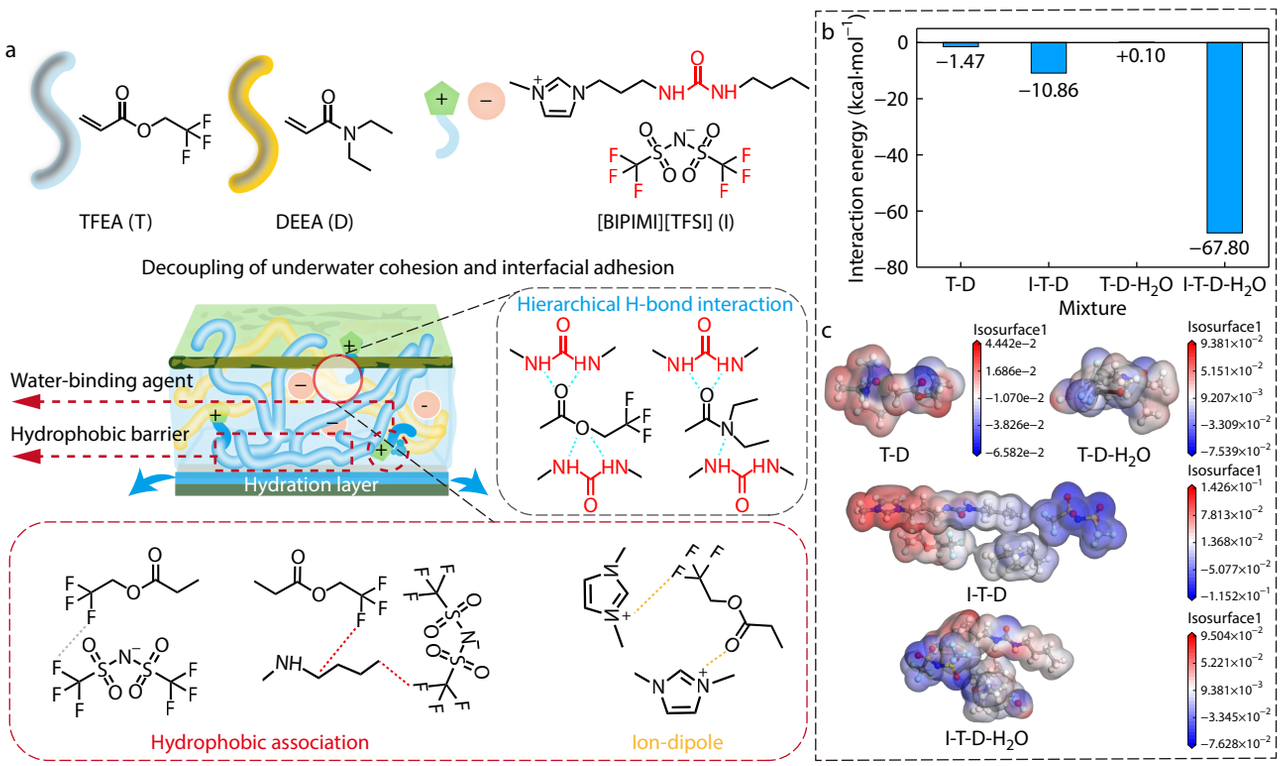


Fig. 1 (a) Schematic illustration of the molecular structure and intermolecular interactions of the ITD ionogel; (b) The calculated interaction energy of the components in the ITD ionogel based on the density functional theory (DFT) optimized structures; (c) The electrostatic potential diagram of T-D, T-D-H_2O, I-T-D, and I-T-D-H_2O pairs.

teractions upon the incorporation of the amphiphilic urea-functionalized IL.

To achieve a deeper understanding of the microstructural stability and water resistance of the ITD ionogel, we further evaluated the interaction energies and electrostatic potential (ESP) maps of the components (IL, monomers, and H_2O). TFEA and DEEA monomers with fluorinated and alkyl groups formed a highly hydrophobic network. Notably, the interaction energy of the monomer-water mixture (T-D-H_2O) revealed a near-zero value of +0.10 kcal·mol^{-1}. This finding supports the strong macroscopic hydrophobic characteristics of T-D polymers, which significantly hinder the infiltration of bulk water molecules and their plasticizing effect on the polymeric networks. When an amphiphilic IL is introduced, the highly polar urea and $TFSI^-$ groups of the IL act as localized water-binding agents. They establish strong hydrogen bonds and ion-dipole interactions with infiltrating water molecules, turning the overall interaction strongly attractive (−67.80 kcal/mol), while the I-T-D network itself maintains a stable cohesive energy of −10.86 kcal·mol^{-1}. These results suggest that the strongly polar motifs of the IL effectively sequester infiltrating water molecules without disrupting the hydrophobic polymeric networks. The ESP map (Fig. 1c) visually confirms that the IL functions as a water-binding agent by capturing water molecules to neutralize their strong polarity. This localized water-scavenging mechanism efficiently removed free water from the adhesive interface while protecting the primary cohesive network from disintegration, thereby ensuring that the ionogel retained its robust mechanical and adhesive properties even under underwater immersion.

Fourier-transform infrared spectroscopy (FTIR) was used to systematically investigate supramolecular interactions within the internal cross-linked network of the ionogels. As shown in Figs. 2(a) and 2(b), the incorporation of DEEA into the ionogel results in notable shifts in the stretching vibration peaks of C—N (1262–1196 cm^{-1}) and C=O (1756–1739 cm^{-1}). These results indicated that DEEA promoted the formation of robust urea-amide hydrogen bonds within the cross-linked network. Furthermore, upon the introduction of the ILs, significant shifts are observed in the stretching vibration bands of C=O (1749–1738 cm^{-1}) and N—H (3309–3291 cm^{-1}), demonstrating the formation of strong urea-amide and urea-ester hydrogen bonds between the IL and the polymeric cross-linked network (Figs. 2c and 2d). Additionally, when TFEA is added, the stretching vibration bands of C—F (1121–1200 cm^{-1}) and C=O (1738–1727 cm^{-1}) exhibit prominent shifts, indicating the establishment of robust hydrophobic associations and ion-dipole interactions within the cross-linked networks (Figs. 2e and 2f).

X-ray photoelectron spectroscopy (XPS) was employed to elucidate the non-covalent interactions within the cross-linked network (Figs. 2g and 2h). As illustrated in Fig. 2(g), the high-resolution C 1s spectrum of the $I_{0\%}T_1D_2$ polymer reveals characteristic peaks corresponding to C—F (292.57 eV), C=O (287.27 eV), C—O/C—N (285.69 eV), and C—C (284.54 eV). Following the incorporation of ILs, the characteristic peaks corresponding to the C—C (284.62 eV), C—O/C—N (286.98 eV), and C=O (288.62 eV) bonds in the $I_{20\%}T_1D_2$ sample shifted to higher binding energies, while the C—F peak (292.33 eV) shifted to a lower binding energy. Fig. 2(h) compares the

https://doi.org/10.1007/s10118-026-3842-z

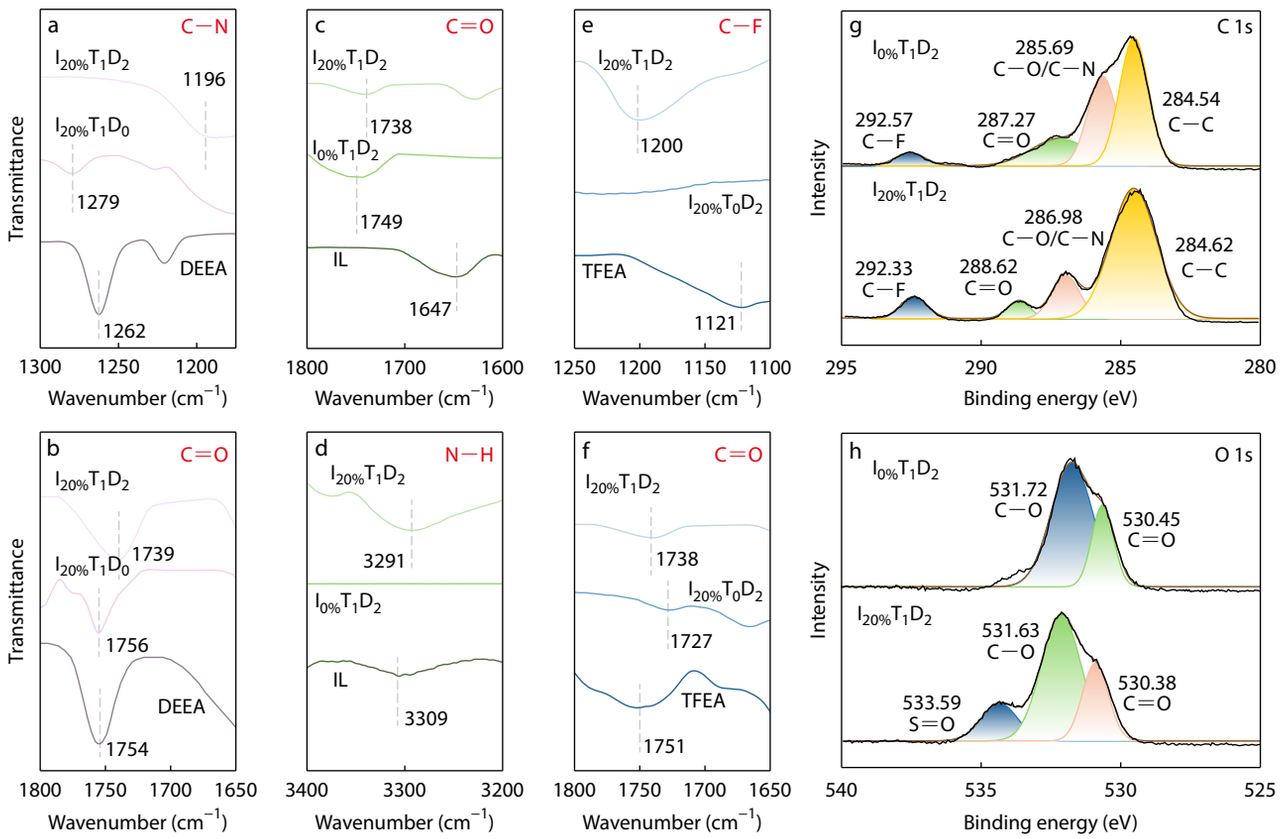


Fig. 2 Characterization of the supramolecular interactions in the ionogel adhesives. (a–f) FTIR spectra of the ionogel, polymer, and monomer; XPS (g) C 1s and (h) O 1s spectra of $I_{0\%}T_1D_2$ and $I_{20\%}T_1D_2$.

high-resolution O 1s spectra of $I_{0\%}T_1D_2$ and $I_{20\%}T_1D_2$. Notably, the $I_{20\%}T_1D_2$ ionogel displayed an additional S=O characteristic peak at 533.59 eV, along with shifts of both the C—O and C=O peaks toward lower binding energies. Collectively, these results corroborate the presence of hierarchical hydrogen bonds, hydrophobic associations, and ion-dipole interactions within the ionogel networks (Fig. 1).

Microstructures of Adhesive Ionogels

As depicted in Fig. 3(a), ionogels with varying compositions (thickness: 0.5 mm) exhibit macroscopic transparency; however, detailed optical transmittance data (Figs. 3b and 3c) reveal a significant composition-dependent hierarchical microphase-separation mechanism. Specifically, the $I_{0\%}T_1D_2$ copolymer without IL exhibited significant macroscopic opaqueness with a transmittance of only about 60% (Fig. 3c), and increasing the hydrophobic TFEA content further diminished the transparency progressively to 59% (Fig. 3b). This opaqueness originates intrinsically from the thermodynamic incompatibility between the highly hydrophobic fluorinated TFEA segments and polar amide DEEA segments, which drives the TFEA segments to associate and form large light-scattering aggregates. Conversely, the introduction of the amphiphilic IL dramatically reversed this trend, increasing the transmittance to over 90% when the IL content reached 50% (Fig. 3c). This enhancement is likely attributed to the strong hydrogen bonding interactions formed between the urea groups in the IL and the amide groups in the polymeric network. Concurrently, the $TFSI^-$ anions establish hydrophobic associations with the fluorine-containing groups in TFEA and ethyl groups in DEEA. These interactions promote uniform dispersion of the IL within the cross-linked polymeric networks, thereby increasing the macroscopic transmittance. Consequently, the IL acts as an effective molecular interfacial compatibilizer that significantly lowers the interfacial tension between the inherently incompatible polymer segments. This compatibilization restricts the TFEA-rich hydrophobic domains to nanoscale dimensions, effectively suppressing macroscopic light scattering, and ultimately yielding highly transparent cross-linked ionogel networks.

Scanning electron microscopy (SEM) was used to examine the evolution of the microstructures of ionogels with different compositions. Fig. 3(d) shows that the SEM image of $I_{20\%}T_0D_1$ exhibits a uniform and smooth surface morphology, while its excellent compositional compatibility contributes to its high macroscopic transparency. In contrast, when the mass ratio of TFEA:DEEA was increased to 2:1, the $I_{20\%}T_2D_1$ ionogel exhibited a distinct microphase-separated morphology in its SEM image, despite remaining macroscopically transparent. This observation directly confirms that the intrinsic incompatibility between copolymer segments induces microphase separation, which is effectively restricted to the nanoscale within the cross-linked network. Fig. 3(e) illustrates that $I_{20\%}T_1D_2$ and $I_{50\%}T_1D_2$, with different IL contents, exhibit distinctly uniform and smooth morphologies, aligned with the high-transmittance results shown in Fig. 3(d). As shown in Fig. S3 (in ESI), the XRD patterns of all ionogels with varying monomer and IL contents displayed two diffraction patterns with broad peaks at $2\theta \approx 8°$ and 20°, indicating the amorphous

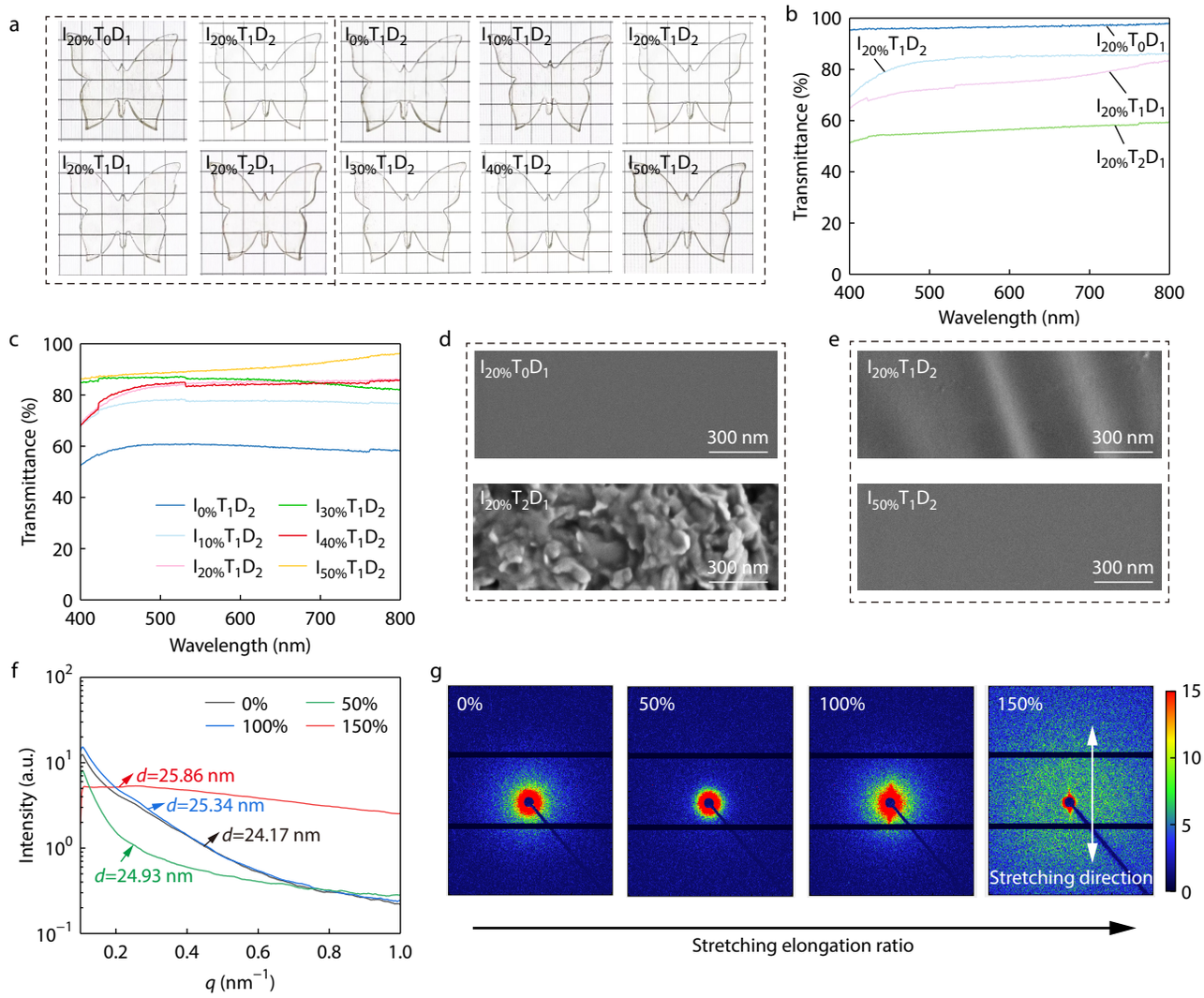


Fig. 3 Microstructural characterization of the ionogel adhesive. (a) Photographs, (b, c) UV transmittance spectra, surface SEM images of (d) $I_{20\%}T_xD_y$ and (e) $I_aT_1D_2$ ionogels with varying compositions; (f) 1D SAXS and (g) 2D SAXS patterns of $I_{20\%}T_2D_1$ ionogel with different stretching elongation ratios.

nature of the ionogels. As illustrated in Fig. 3(f), a weak scattering peak appeared at approximately 0.26 nm^{-1} in the SAXS curves of the $I_{20\%}T_2D_1$ ionogel, which was attributed to scattering resulting from microphase separation. Upon applying uniaxial strain from 0% to 150%, the scattering peak gradually shifted to a lower q value of 0.24 nm^{-1}, indicating an increase in the characteristic spacing of the microphase-separated domains along the stretching direction. Furthermore, pronounced changes were evident in the SAXS data, indicating the dynamic structural evolution of the microphase-separated network under stress.[27] Specifically, at an initial strain of 50%, the originally isotropic domains begin to yield, undergoing significant plastic deformation and orientation along the macroscopic stretching direction, which causes an abrupt change in the scattering profile. Furthermore, when the strain reached 150%, the polymer chains between the cross-linking points became highly extended and closely packed. This stress-induced structural densification substantially amplifies the electron density contrast ($\Delta\rho$) between the separated copolymer phases. According to the X-ray scattering theory, this enhanced $\Delta\rho$ directly manifests as a sharp increase in the scattering spot intensity in the 2D-SAXS patterns. As shown in Fig. 3(g), the 2D-SAXS patterns evolved from an isotropic ring into highly anisotropic elliptical shapes. The scattering signal became significantly stronger in the equatorial direction (perpendicular to the stretching axis), with the eccentricity increasing at higher elongation ratios. Ultimately, this unique strain-responsive microphase-separated architecture provides a robust energy-dissipation mechanism at multiple scales, thereby conferring excellent mechanical toughness to the ionogel.

Mechanical and Adhesive Properties of Adhesive Ionogels

To systematically elucidate the underlying mechanisms by which the composition of ionogels influences their mechanical and adhesion properties, we conducted mechanical and lap-shear tests on ITD ionogels with varying monomer and IL content. As illustrated in Figs. 4(a) and 4(b), increasing the TFEA/DEEA mass ratio results in a gradual decrease in the ten-

https://doi.org/10.1007/s10118-026-3842-z

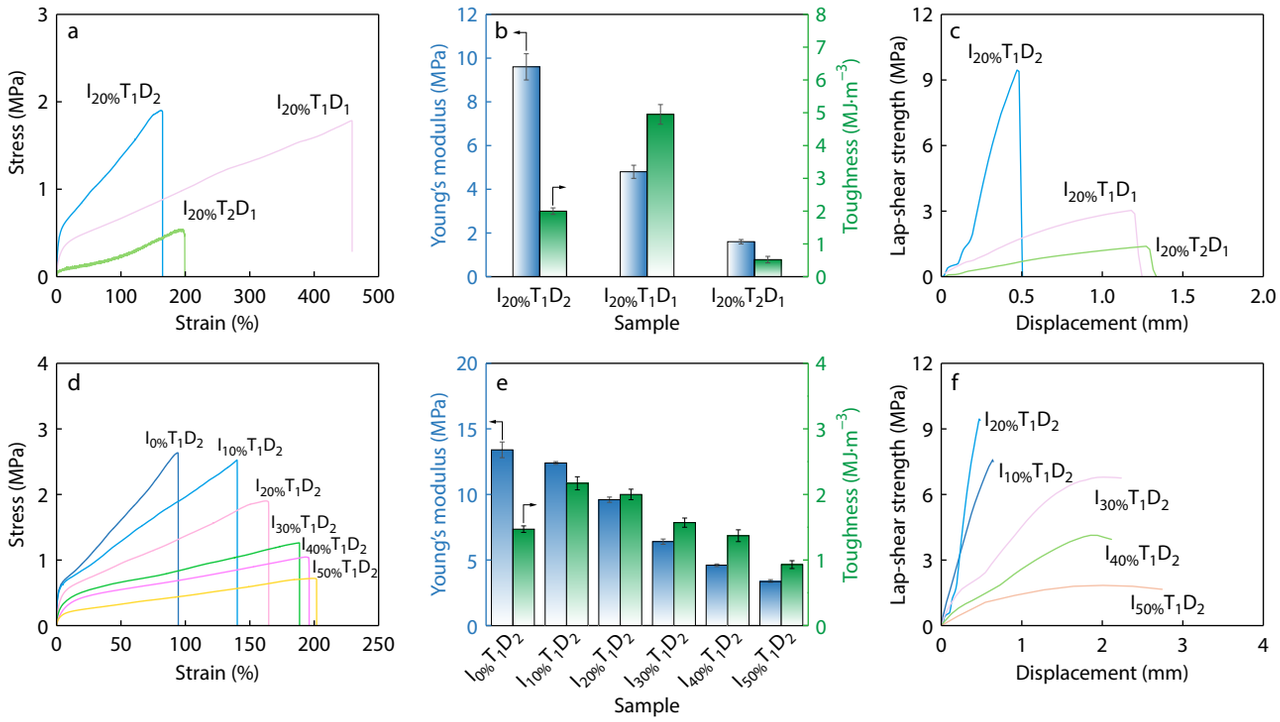


Fig. 4 Mechanical and adhesive properties of the ionogel adhesive. (a) Stress-strain curves, (b) Young's modulus and toughness, and (c) lap-shear strength–displacement curves of sample $I_{20\%}T_xD_y$ ionogels; (d) Stress-strain curves, (e) Young's modulus, and toughness, and (f) shear strength–displacement curves of $I_aT_1D_2$ ionogels adhesive to the glass substrate.

sile strength of $I_{20\%}T_xD_y$ ionogels, from 1.89 MPa to 0.49 MPa. The elongation at break ranges from 164% to 458%, and both the Young's modulus and toughness exhibit declining and nonlinear trends, respectively, with toughness initially increasing before decreasing. These results may be attributed to the introduction of TFEA, which progressively transforms the relatively strong intermolecular amide-urea hydrogen bonding interactions within the ionogel network into weaker hydrophobic associations and dipole-dipole interactions, thereby reducing the rigidity of the molecular chains. This transition in internal molecular interactions also profoundly impacts interfacial adhesion. As shown in Fig. 4(c), the lap-shear strength on glass substrates declines sharply from 9.44 MPa to 1.03 MPa as the TFEA content increases. Interestingly, this decline in adhesion reveals a highly insightful correlation with macroscopic optical opacity (Fig. 3b), highlighting a critical structure-property trade-off for practical wearable sensors. Specifically, higher TFEA contents drive a more pronounced microphase separation, which leads to optical opaqueness and concurrently dilutes the density of active hydrogen-bonding sites available to interact with substrates. Consequently, an increase in macroscopic optical opacity serves as a direct indicator of diminished microscopic interfacial adhesion. Through a comprehensive evaluation of the intricate balance between mechanical robustness, interfacial adhesion, and optical transparency, the $I_{20\%}T_1D_2$ ionogel was identified as the optimal formulation, achieving a notable adhesion strength of 9.44 MPa, along with favorable mechanical properties (1.89 MPa, 164%) and good transparency (80%). Therefore, the TFEA/DEEA mass ratio was maintained at 1:2 for subsequent investigation of the effects of the IL content.

As depicted in Fig. 4(d), the $I_{0\%}T_1D_2$ polymer without the IL exhibited pronounced brittleness and lacked adhesion properties. Increasing IL content from 10% to 50% leads to a reduction in the fracture strength of $I_aT_1D_2$ ionogels, from 2.52 MPa to 0.71 MPa, while the elongation at break progressively increases. As illustrated in Fig. 4(e), the Young's modulus of the $I_aT_1D_2$ ionogels decreased with increasing IL content, and toughness showed a trend of first increasing and then decreasing, with $I_{20\%}T_1D_2$ achieving the highest toughness of 4.95 MJ·m^{-3}. This behavior is attributed to the synergistic effect between the increase in bidentate urea hydrogen bonds within the ionogel network facilitated by the IL introduction and the plasticizing effect of the IL. Fig. 4(f) shows that, as the IL mass fraction increases from 0% to 20%, the lap shear strength sharply increases to 9.44 MPa, subsequently declining to 1.83 MPa for $I_{50\%}T_1D_2$. These findings indicated that the IL content significantly influenced the adhesion properties of the $I_aT_1D_2$ ionogels. This result corroborates with the DFT calculations. The introduction of an optimal IL concentration effectively dissociated and reconstructed the polymer network, liberating numerous free hydrogen-bonding groups and enhancing the adhesion performance at the substrate interface.

In summary, both the TFEA/DEEA mass ratio and the IL content significantly influenced the mechanical and adhesion properties of the ionogels. The tensile strength (0–2.52 MPa), lap shear strength on glass substrates (0–9.44 MPa), Young's modulus (0–13 MPa), and toughness (0–4.95 MJ·m^{-3}) can be finely tuned over a wide window. The rational design of the molecular structure endows the ionogels with superior mechanical and adhesion properties, facilitating the effective decoupling of bulk cohesion and interfacial adhesion. Notably, the $I_{20\%}T_1D_2$ ionogel exhibited exceptional mechanical (1.89

MPa, 164%) and adhesion properties (9.44 MPa), significantly surpassing most instant-adhesion ionogel systems reported in recent literature (Table S2 in ESI).[28–33] This demonstrates broad application prospects in flexible electronics, tissue adhesives, and wearable devices.

Underwater Adhesion Performances of the Ionogels

The adhesion strength of the $I_{20\%}T_1D_2$ ionogel adhesive to the glass substrates in air reached a remarkable 9.44 MPa. As illustrated in Fig. 5(a), a glass assembly with an adhesion area of approximately 5 cm^2 is capable of suspending a 50 kg water bucket in air and successfully maintaining the structural integrity of the bonded assembly without debonding when submerged in water, demonstrating the exceptional adhesion performance of the ionogel in air and outstanding stability in aqueous environments. As shown in Fig. S4 (in ESI), when the soaking time of the $I_{20\%}T_1D_2$ ionogel adhesive in water was extended to 8 days, its mass gradually increased to 111% of its initial value, indicating good hydrophobic properties and water resistance. As depicted in Figs. 5(b) and 5(c), after an 8-day immersion in water, the $I_{20\%}T_1D_2$ ionogel retained over 90% of its initial mechanical strength and lap-shear strength, confirming its excellent interfacial water-repelling capability and long-term underwater stability. This result corroborates with our microscale DFT calculations (Fig. 1). Specifically, the near-zero interaction energy (+0.10 $kcal·mol^{-1}$) between the T-D polymeric network and water confirms that the dense fluorinated/alkyl segments serve as a thermodynamic barrier, effectively repelling bulk water infiltration. Concurrently, the strong attractive interaction energy (–67.80 $kcal·mol^{-1}$) in the I-T-D-H_2O system indicates that the highly polar motifs of the IL act as potent water-binding agents. This synergistic effect efficiently entrapped interfacial trace water molecules, thus completely shielding the primary cohesive hy-

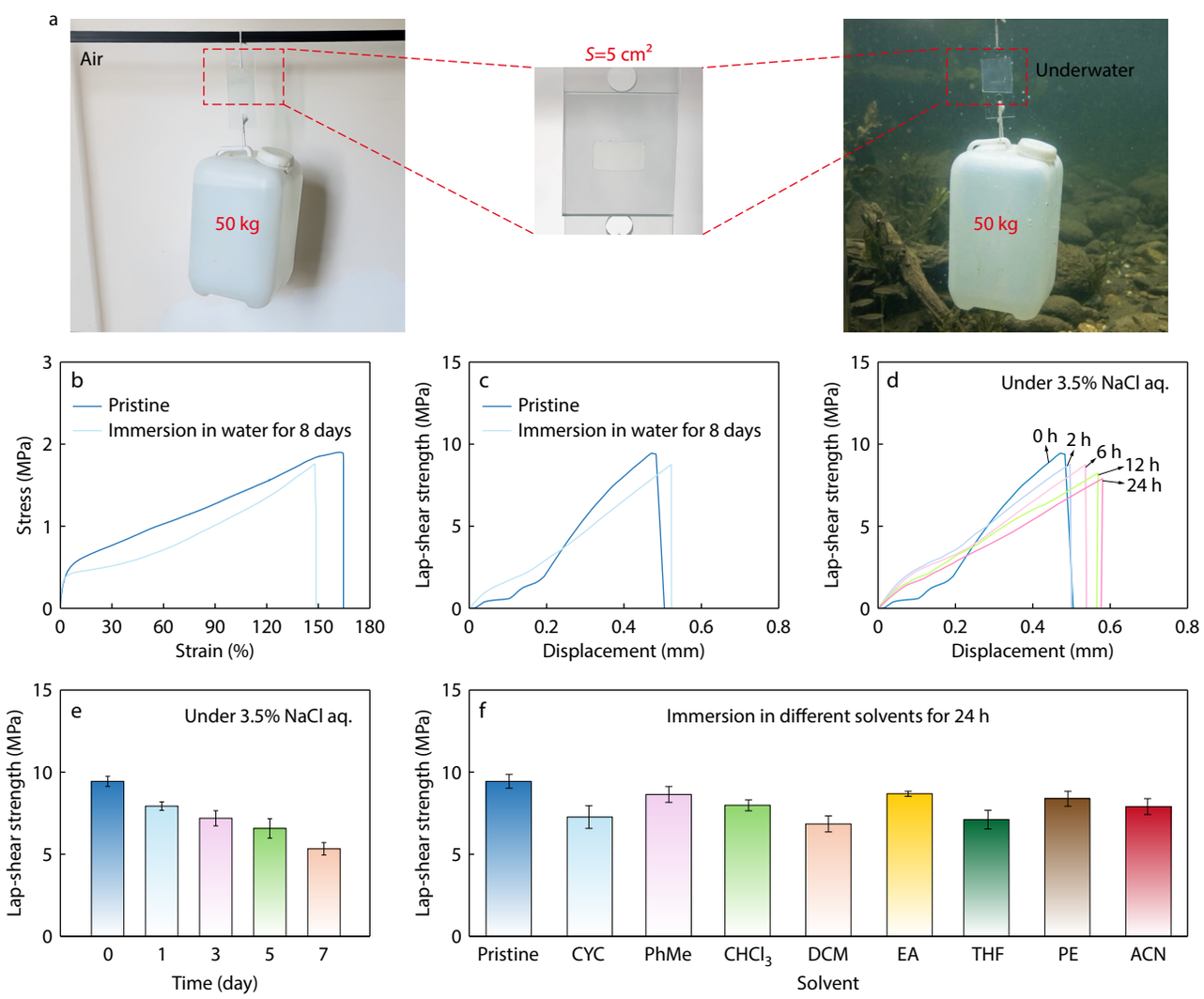


Fig. 5 Underwater adhesion and adhesive stability of the $I_{20\%}T_1D_2$ ionogel adhesive. (a) Photographs demonstrating the macroscopic load-bearing capability of the ionogel in air lifting a 50 kg water bucket and its structural integrity without debonding when entirely submerged in water; (b) Stress-strain curves, and (c) lap-shear strength-displacement curves of the $I_{20\%}T_1D_2$ ionogel after immersion in water for 8 days; (d) Lap-shear strength-displacement curves of the $I_{20\%}T_1D_2$ ionogel upon immersion in a 3.5% NaCl simulated seawater solution for 24 h; (e) The variations of lap-shear strength of $I_{20\%}T_1D_2$ ionogel upon immersion in simulated seawater over time; (f) Lap-shear strength of $I_{20\%}T_1D_2$ ionogel upon immersion in various solvents for 24 h.

https://doi.org/10.1007/s10118-026-3842-z

drogen-bonding network from hydration-induced plasticization. This results in successful decoupling of the underwater bulk cohesion and interfacial adhesion.

Fig. 5(d) illustrates that following immersion of the $I_{20\%}T_1D_2$ ionogel in a 3.5% NaCl solution (simulated seawater) for 24 h, the lap-shear strength gradually decreases from 9.44 MPa to 7.87 MPa. Furthermore, after being submerged in simulated seawater for seven days, the adhesion strength still reaches 5.33 MPa (Fig. 5e and Fig. S5 in ESI). This further substantiates their exceptional interfacial water repulsion and underwater stability. This can be attributed to several factors. Firstly, the hydrophobic interactions among the $TFSI^-$ anions, alkyl chains, and C—F chains within the cross-linked network effectively repel water molecules and disrupt the interfacial hydration layer; secondly, the high-density hierarchical hydrogen bonds and electrostatic interactions formed between the ionogel and the glass substrate confer superior adhesion performance. Moreover, the Im^+ cations in ILs effectively compete with and displace hydrated salt ions on the substrate surface, thereby establishing robust interfacial adhesion in a simulated seawater environment.[34,35] This lays a solid foundation for the application of ionogels in fields such as underwater equipment sealing and marine wearable sensors.

As depicted in Fig. 5(f), due to the extremely low solubility of the $I_{20\%}T_1D_2$ ionogel in organic solvents, its adhesion strength on glass substrates remains over 6.5 MPa (retaining over 68% of the initial adhesive strength) after being immersed for 24 h in solvents such as cyclohexane (CYC), toluene (PhMe), chloroform ($CHCl_3$), dichloromethane (DCM), ethyl acetate (EA), tetrahydrofuran (THF), petroleum ether (PE), and acetonitrile (ACN), demonstrating excellent solvent resistance.

Multifunctionality of Adhesive Ionogels

Hierarchical hydrogen and hydrophobic associations present within ITD ionogels exhibit reversible breaking and recombination in response to external stimuli, thereby imparting a variety of functionalities to the materials, including self-healing, self-welding, and recyclability. This versatility significantly extends the service life of the materials and augments their durability.[36–38] As illustrated in Fig. 6(a), two dumbbell-shaped specimens, dyed blue and yellow, respectively, were severed. The cut surfaces achieved self-healing at 40 °C over a duration of 24 h without external pressure, and the healed specimen demonstrated the ability to be stretched by up to 125%. As shown in Fig. 6(b), after the specimen was severed, the edges were immediately overlapped and placed between two glass

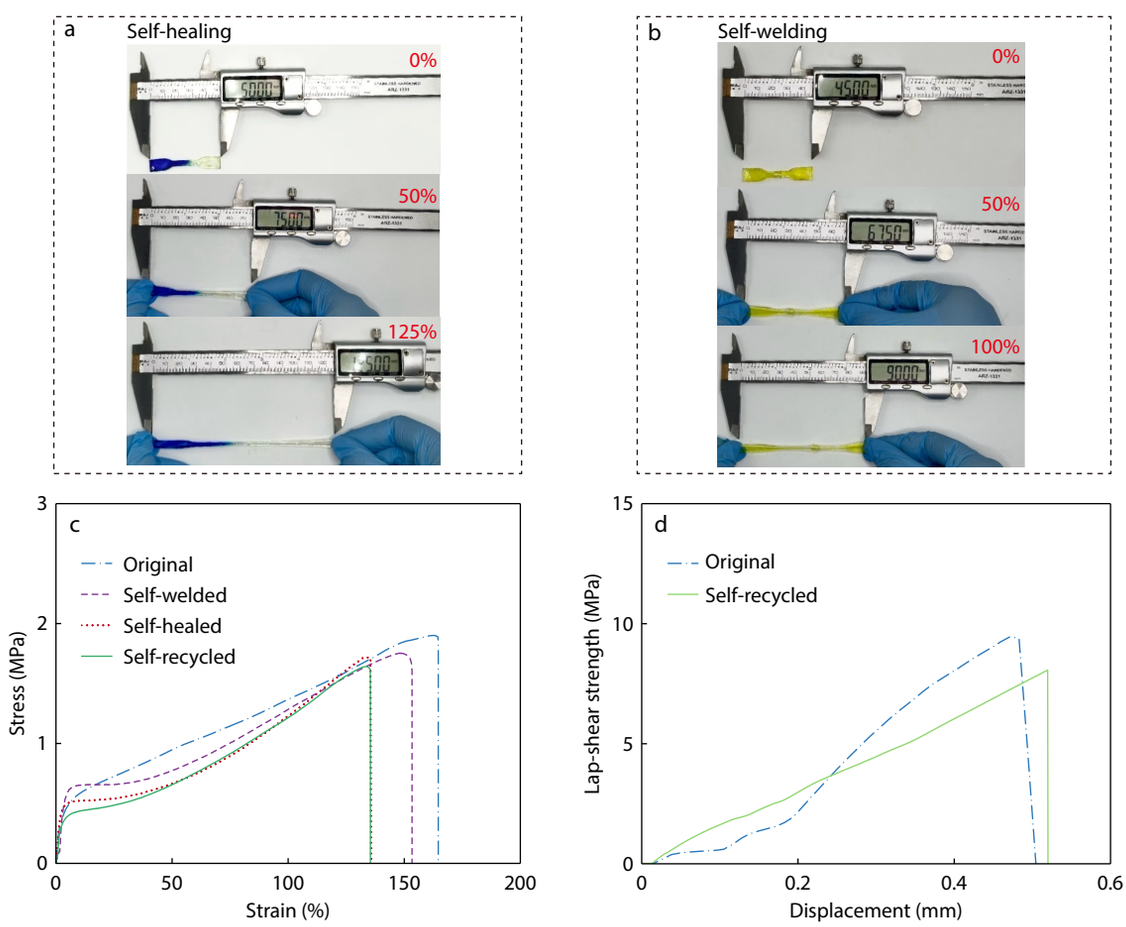


Fig. 6 Multifunctionality of the $I_{20\%}T_1D_2$ adhesive ionogel. (a) Stretching photographs of the $I_{20\%}T_1D_2$ ionogel after self-healing at 40 °C; (b) Stretching photographs of the $I_{20\%}T_1D_2$ ionogel after self-welding at 40 °C; (c) Stress-strain curves of the $I_{20\%}T_1D_2$ ionogel after self-healing/welding at 40 °C for 24 h and self-recycling in ethanol; (d) Lap-shear strength-displacement curves of the $I_{20\%}T_1D_2$ ionogel after self-recycling in ethanol.

https://doi.org/10.1007/s10118-026-3842-z

plates. Under the same conditions, the self-welded specimen could be stretched to 100%. As depicted in Fig. 6(c), the I20%T1D2 ionogel exhibits exceptional self-healing and self-welding efficiencies of 92% and 94%, respectively. The exceptional self-healing/welding properties of the I20%T1D2 ionogel at mild 40 °C can be primarily attributed to the enhanced mobility of molecular chains and the increased chain diffusion rate at this temperature, which facilitates the rapid fusion of molecular chains at fractured or overlapping surfaces. Furthermore, the rapid dissociation and recombination of dynamic physical cross-links within the network enable the cross-linked network to achieve complete healing and welding.

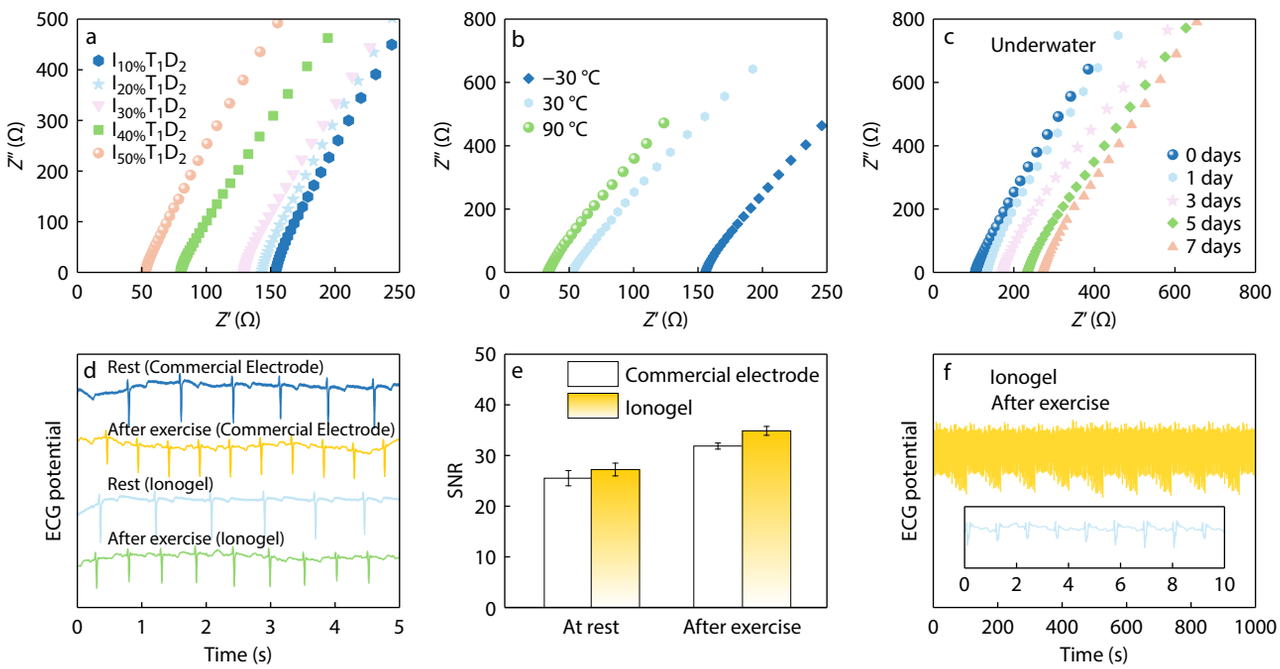
The discarded ionogel was cut into small pieces and immersed in ethanol. After stirring at room temperature for 24 h, ionogel was completely dissolved in ethanol. The resulting solution was poured into a dumbbell-shaped mold, and after evaporation of the solvent, a new recycled specimen was formed. As demonstrated in Figs. 6(c) and 6(d), the mechanical strength of the recycled specimen retained 88% of that of the original specimen, while its lap-shear strength maintained 84% of its original value, indicating excellent recyclability. This result is attributed to the strong hydrogen bonding interactions between ethanol and the ionogels, which competitively disrupt the intermolecular hydrogen bonds between polymer chains, thus enabling complete dissolution of the ionogel in ethanol and endowing the ionogel with exceptional recyclability.

Physiological Signal Monitoring of Adhesive Ionogels

Fig. 7(a) illustrates the electrochemical impedance spectroscopy (EIS) profile of the $I_aT_1D_2$ ionogels with different contents of ILs at room temperature. Correspondingly, the $I_{20\%}T_1D_2$ ionogel exhibited an initial ionic conductivity of 0.0175 S/m. As depicted in Fig. 7(b), the ionic conductivity of the $I_{20\%}T_1D_2$ ionogel demonstrates a significant increase from 0.0166 $S{\cdot}m^{-1}$ to 0.0754 $S{\cdot}m^{-1}$ with rising temperature from −30 °C to 90 °C. At 90 °C, the conductivity reaches 0.0754 S/m, which is 4.3 times that observed at 30 °C. Following immersion in water, the resistance gradually increased, resulting in a conductivity decline to 0.00637 $S{\cdot}m^{-1}$ (Fig. 7c). After extended immersion time, the conductivity gradually stabilizes, indicating robust ion transport performance in underwater environments.

Considering that the $I_{20\%}T_1D_2$ ionogel exhibited optimal characteristics, including high conductivity, underwater conductive stability, flexibility, and transparency, it was selected as the ideal candidate for assessing sensing performance. To record human electrocardiogram (ECG) signals, $I_{20\%}T_1D_2$ electrodes (25 mm × 25 mm × 2 mm) were affixed to the human chest and connected to a BMD101 module using conductive wires. The recorded ECG signals were transmitted *via* Bluetooth to a computer equipped with the BMD101 ECG monitoring software. To validate the accuracy of the $I_{20\%}T_1D_2$ electrodes in monitoring ECG signals, built-in commercial electrodes of the ECG tester were employed to record human ECG in a relaxed state for comparative analysis. As illustrated in Figs. 7(d) and 7(e), each waveform in the ECG trace collected by the $I_{20\%}T_1D_2$ electrodes was complete, continuous, and stable. Exercise-related increases in the heart rate resulted in a decreased interval between consecutive ECG waveforms, demonstrating strong comparability with the results from the commercial ECG tester. Additionally, as presented in Fig. 7(f), to further verify the long-term stability of the $I_{20\%}T_1D_2$ electrodes in capturing ECG signals, continuous variations in human ECG signals over 16 min were recorded. The results indicate that the ECG signals maintain good stability over time, confirming the substantial potential of the $I_{20\%}T_1D_2$ electrode for monitoring human ECG signals.

Electromyography (EMG) signals reflect electrical signals generated by muscle contractions and provide essential information for assessing human muscle activity.[39–41] The $I_{20\%}T_1D_2$ electrodes were applied to the biceps brachii of the



https://doi.org/10.1007/s10118-026-3842-z

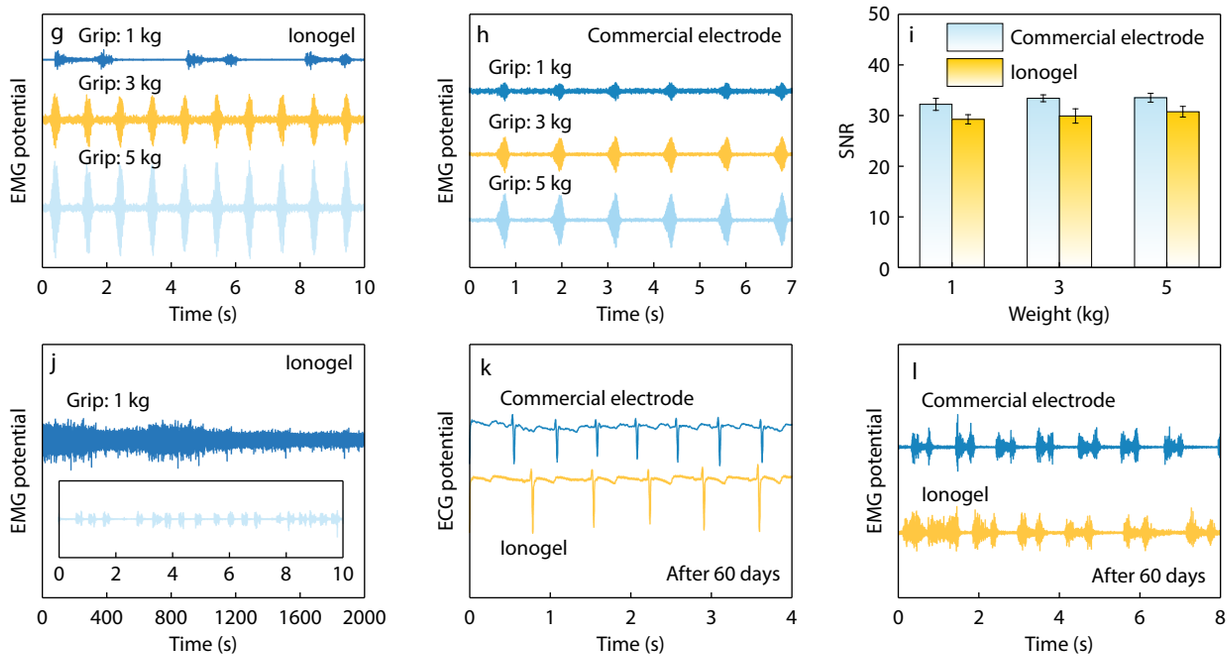


Fig. 7 Applications of the $I_{20\%}T_1D_2$ ionogel adhesive in electrochemical performance and electrophysiological signal monitoring. (a) Electrochemical impedance spectra (EIS); (b) EIS of $I_{20\%}T_1D_2$ ionogel at different temperatures; (c) EIS of $I_{20\%}T_1D_2$ upon immersion in water for different time; Comparison of ECG signals (d) and signal-to-noise ratios (SNRs) (e) recorded by the commercial electrode and $I_{20\%}T_1D_2$ at rest and during motion; (f) ECG signals of $I_{20\%}T_1D_2$ for over 16 min after exercise; Comparison of EMG signals (g, h) and SNRs (i) recorded by the commercial electrode and $I_{20\%}T_1D_2$ upon lifting weights; (j) EMG signals of $I_{20\%}T_1D_2$ for over 30 min of lifting a 1 kg weight; Comparison of ECG signals after exercise (k) and EMG signals upon lifting of 1 kg weight (l), recorded by a used commercial electrode and $I_{20\%}T_1D_2$ after 60 days of storage.

human arm, whereas the reference electrode was attached to the wrist to record EMG signal variations under different load conditions. Simultaneously, the built-in commercial electrodes of the EMG tester were used to record the EMG signals. As depicted in Figs. 7(g)–7(i), with increasing lifting weight, the intensity of muscle contractions increases, leading to a corresponding enhancement in the amplitude of EMG signals. This result indicates that the $I_{20\%}T_1D_2$ electrode responds sensitively to electrophysiological changes associated with muscle activity, producing results comparable to those obtained using the commercial EMG tester. Furthermore, as shown in Fig. 7(j), continuous EMG signals were recorded over 30 min under a 1 kg load using the $I_{20\%}T_1D_2$ electrode. Additionally, ECG and EMG signals were recorded using the same ionogel electrode on 1st and 60th days, respectively (Figs. 7k and 7l). The recordings from the 60th day were obtained using the previously employed $I_{20\%}T_1D_2$ electrode, which was stored under ambient conditions for 60 days. The findings demonstrate that both the ECG and EMG signals exhibit excellent stability over an extended period. Therefore, the $I_{20\%}T_1D_2$ electrode could accurately and reliably record human ECG and EMG signals.

CONCLUSIONS

In summary, we successfully developed mechanically robust and multifunctional underwater adhesive ionogels using a supramolecular design strategy that exploits synergistic hierarchical hydrogen bonding and hydrophobic associations. The optimized ionogel exhibited exceptional tensile strength (1.89 MPa and impressive lap-shear strength (9.44 MPa, maintaining over 90% of the mechanical and adhesive strength upon immersion in water for 8 days. DFT calculations confirmed the synergistic effect of the fluorinated hydrophobic barrier and the water-binding agent of ILs, effectively entrapping infiltrating trace water molecules, contributing to the decoupling of underwater bulk cohesion and interfacial adhesion. Furthermore, the dynamic reversibility of supramolecular networks imparts ionogels with highly efficient self-healing and self-welding capabilities (>90%) at a mild temperature of 40 °C along with excellent ethanol-assisted recyclability. Ultimately, the ionogel electrodes were successfully deployed for the highly stable real-time monitoring of human electrophysiological signals. By bridging the gap between extreme environment adhesion and dynamic sustainability, this study presents a compelling material platform for next-generation wearable healthcare devices and advanced marine bioelectronics.

Conflict of Interests

The authors declare no interest conflict.

Electronic Supplementary Information

Electronic supplementary information (ESI) is available free of charge in the online version of this article at http://doi.org/10.1007/s10118-026-3842-z.

Data Availability Statement

The related data of this paper are data that should not be

shared and can be obtained from the author for reasonable reasons. Author contact information: chm_leil@ujn.edu.cn.

ACKNOWLEDGMENTS

This work was financially supported by the Natural Science Foundation of Shandong Province (Nos. ZR2021ME055 and ZR2022QB170), the Research Project for Newly Introduced Talents of the University of Jinan (No. XBS2418), and the Key Research and Development Program of Shandong Province (Nos. 2026CXPT119, 2025TSGCCZZB0394 and 2024TSGC0909).

REFERENCES

1 Zhang, Z. Y.; Yao, A. F.; Raffa, P. Transparent, highly stretchable, self-healing, adhesive, freezing-tolerant, and swelling-resistant multifunctional hydrogels for underwater motion detection and information transmission. *Adv. Funct. Mater.* **2024**, *34*, 2407529.
2 Jiao, B.; Wang, W.; Feng, Y.; Zhou, D.; Wang, X.; Zhou, Y.; Wang, X.; Shang, Y.; Wang, Q. High-strength liquid metal composite–hydrogel interfaces enable robust stretchable electronics. *Nat. Commun.* **2026**, *17*, 5322.
3 Li, Z. J.; Xie, W. C.; Zhao, T. N.; Li, Y. Z.; Mao, Z. H.; Ye, X. F.; Fan, C. H.; Zhang, Z. T. Highly conductive ag flakes-based bio-adhesive for multi-functional epidermal electronics. *Adv. Mater.* **2026**, *38*, e21677.
4 Yu, J. J.; Xiong, J. F.; Wu, B. Y.; Ma, Q.; Zhang, S. L.; Wang, J. Y.; Wang, X. W.; Li, W. Z.; Yan, F. Bio-ionic liquid-induced rapid self-initiating tough ionogels for in situ adhesion. *Adv. Mater.* **2026**, e73565.
5 Liu, L. L.; Liu, Z. Y.; Ren, Y. Y.; Zou, X. Y.; Peng, W. S.; Li, W. Z.; Wu, Y. Q.; Zheng, S. J.; Wang, X. L.; Yan, F. A Superstrong and reversible ionic crystal-based adhesive inspired by ice adhesion. *Angew. Chem. Int. Ed.* **2021**, *60*, 8948–8959.
6 Huang, Y. Y.; Ming, X. Q.; Tang, Z.; Chen, G. Q.; Duan, X. Z.; Zhu, H.; Zhu, S. P.; Zhang, Q. Ultra-strong ionogel adhesives via in situ microphase separation. *Adv. Funct. Mater.* **2025**, *35*, 2417011.
7 Zhai, H. L.; Qin, W. J.; Wang, Y. L.; Gu, C. S.; Chen, M. Y.; Ge, L.; Xue, S.; Li, X. X.; Zhao, X. C.; Xu, Y. X.; et al. "Ionic ocean" constructed super underwater adhesive, stretchable, self-healing hydrophobic conductive ionogel. *Adv. Funct. Mater.* **2025**, *35*, 2505171.
8 Ma, B. L.; Yang, Y.; Wang, J. Q.; Yu, Z. C.; Wu, P. Y. Harnessing

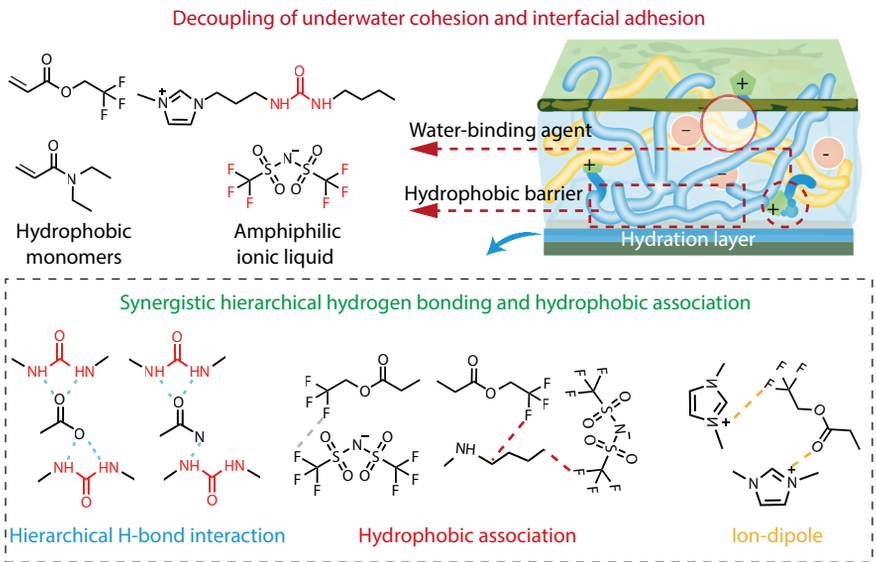
Graphical Abstract

Synergistic Hierarchical Hydrogen Bonding and Hydrophobic Association Enable Mechanically Robust Underwater Adhesive Ionogels for Wearable Sensing

Lan Lei, Xiao-Xuan Liu, Wen-Jie Yang, Yu Xie, Xian-Wen Hong, Yu-Heng Liu, Chun-Jie Xie, Chuan-Yong Zong, and Hui Li

University of Jinan

This work presents an underwater adhesive ionogel that combines mechanical robustness and long-term aquatic stability. The ionogel featured a dynamic supramolecular network comprising synergistic hierarchical hydrogen bonding and hydrophobic associations. This architecture enables exceptional tensile and adhesive strengths, highly efficient self-healing, and high-fidelity wearable monitoring of electrophysiological signals.



Chinese J. Polym. Sci. 2026 *https://doi.org/10.1007/s10118-026-3842-z*

water molecules for strong underwater adhesion. *Adv. Mater.* **2026**, *38*, e73571.
9 Ding, Y.; Xie, J. W.; An, L. F.; Yan, C. C.; Yan, F. Covalent adaptable ionic networks for robust, on-demand dismantlable and fully recyclable adhesives. *Adv. Mater.* **2026**, *38*, e73259.
10 Li, Q. N.; Zheng, S. J.; Liu, Z. Y.; Li, W. Z.; Wang, X. W.; Cao, Q.; Yan, F. Strong, spontaneous, and self-healing poly(ionic liquid) elastomer underwater adhesive with borate ester dynamic crosslinking. *Adv. Mater.* **2024**, *36*, 2413901.
11 Xiong, J. F.; Duan, M. Z.; Zou, X. Y.; Gao, S. N.; Guo, J. N.; Wang, X. W.; Li, Q. N.; Li, W. Z.; Wang, X. L.; Yan, F. Biocompatible tough ionogels with reversible supramolecular adhesion. *J. Am. Chem. Soc.* **2024**, *146*, 13903−13913.
12 Yang, H. L.; Wang, W. Q.; Zhu, C. J.; Chen, G. Q.; Zheng, J. X.; Li, S. N.; Ren, J. Y.; Fu, J. Reversible, ultra-strong underwater adhesive based on supramolecular interaction for instant liquid leakage sealing and robust tissue adhesion. *Chem. Eng. J.* **2024**, *480*, 148064.
13 Yu, J.; Xie, R. L.; Zhang, M. Y.; Shen, K. X.; Yang, Y. X.; Zhao, X. D.; Zhang, X.; Zhang, Y. F.; Cheng, Y. L. Molecular architecture regulation for the design of instant and robust underwater adhesives. *Sci. Adv.* **2023**, *9*, eadg4031.
14 Cheng, B. H.; Yu, J. H.; Arisawa, T.; Hayashi, K.; Richardson, J. J.; Shibuta, Y.; Ejima, H. Ultrastrong underwater adhesion on diverse substrates using non-canonical phenolic groups. *Nat. Commun.* **2022**, *13*, 1892.
15 Xing, Q.; Zhen, L.; Zhou, X. L.; Zhong, S. T.; Li, F. X.; Li, J. Y.; Meng, R. Y.; Duan, P. P.; Luo, J.; Yang, J. J. Cohesion regulation of polyphenol cross-linked hydrogel adhesives: from intrinsic cross-link to designs of temporal responsiveness. *Adv. Funct. Mater.* **2025**, *35*, 2414294.
16 An, S.; Jejeon, E.; Han, S. Y.; Jeon, J.; Lee, M. J.; Kim, S.; Shin, M.; Cho, S. W. pH-Universal catechol-amine chemistry for versatile hyaluronic acid bioadhesives. *Small* **2022**, *18*, 2202729.
17 Wang, W. B.; Wang, Z.; An, Z. X.; Xiao, H. Y.; Teng, P. C.; Wang, S. T. Cation-*π*-driven responsive underwater adhesives with high adhesion switching ratios. *Adv. Funct. Mater.* **2026**, *36*, e16094.
18 Wang, S. X.; Li, J. J.; Li, S.; Wu, X. C.; Guo, C.; Yu, L. M.; Murto, P.; Wang, Z. H.; Xu, X. F. Self-contained underwater adhesion and informational labeling enabled by arene-functionalized polymeric ionogels. *Adv. Funct. Mater.* **2023**, *33*, 2306814.
19 Qi, J.; Xie, X. W.; An, S. C.; Luo, T.; Yu, J.; Zhao, J. K.; Wang, C. P.; Chu, F. X.; Cheng, Z. H.; Wang, J. F. Hydrophobic ionogel with mitigated sea-island structure: exhibiting ultrahigh adhesion *via* cellulose-mediated energy dissipation. *J. Colloid Interf. Sci.* **2026**, *704*, 139459.
20 Zhang, Z. Y.; Yao, A. F.; Raffa, P. Physically crosslinked amphiphilic eutectogels with underwater self-healing, strong adhesion, environmental stability and closed-loop recyclability for underwater sensing and information transmission. *Chem. Eng. J.* **2025**, *522*, 167958.
21 Zhang, Y.; Sun, Y. N.; Yang, J. H.; Tian, R. B.; Liu, J. H.; Tang, X. M.; Wang, J. B.; Li, Q. S. A robust and adhesive anti-swelling hydrophobic ionogel with prolonged stability for strain and temperature sensors. *J. Mater. Chem. A* **2024**, *12*, 33734−33745.
22 Wei, J. J.; Zheng, Y. F.; Chen, T. A fully hydrophobic ionogel enables highly efficient wearable underwater sensors and communicators. *Mater. Horiz.* **2021**, *8*, 2761−2770.
23 Wu, H. R.; Gao, N.; Song, J. X.; Pang, X. L.; Li, Y. J.; Xu, Z. C.; Yu, X. D. Hydrophobic deep eutectic solvent-based hydrophobic polymer adhesive with on-demand detachability and strong broad-spectrum adhesion in air/aquatic environments. *J. Mater. Chem. A* **2025**, *13*, 21629−21640.
24 Wang, W.; Wu, B. H.; Sun, S. T.; Wu, P. Y. Amphibious breathable ionic skin enabled by dynamically interlocked star-shaped ionic liquid telomers. *Adv. Mater.* **2026**, *38*, e73701.
25 Yu, N.; Liu, P. Q.; Lin, Y. L.; Zhang, A. Q. The robustness waterproof ionogel based on the phase separation to form soft hard heterostructures and the interaction of cation-π realizes underwater adhesion and sensing. *Chem. Eng. J.* **2024**, *497*, 155046.
26 Liu, X. X.; Lei, L.; Xie, Y.; Xie, C. J.; Li, H. Thermodynamically driven decoupling of cohesion-adhesion for ultrarobust underwater ionogel adhesives. *Chem. Eng. J.* **2026**, *536*, 175901.
27 Noh, S.; Sugawara, A.; Ishihara, N.; Konishi, T.; Ueda, Y.; Motokawa, R.; Takashima, Y.; Uyama, H. Real-time stress visualization of hydrogels enabled by supramolecularly switched stretch-induced phase separation. *Adv. Sci.* **2026**, e76110.
28 Chen, S. Q.; Wang, Q. H.; Shao, J. W.; Li, X. Y.; Bian, Y. Y.; Jiang, S. C.; Cao, Z. Q.; Li, J. Z. Decoupling of bonding strength and water retention in aqueous wood adhesive inspired by plant cell. *ACS Nano* **2025**, *19*, 15876−15885.
29 Chen, X. Y.; Ming, X.; Wang, J. X.; Xia, Z. H.; Zhu, X.; He, L.; Feng, X. Y.; Fang, W. Z.; Huang, L.; Xu, Z.; Peng, Y. X. Underwater instant adhesive hydrogel interfaces for robust biosensing on diverse species. *Adv. Sci.* **2025**, *12*, e10702.
30 Ma, H. Y.; Wu, C.; Ma, H. X.; Liu, X. F.; Ma, T.; Xia, Z. M.; Liu, X.; Zhang, X.; Zhang, H. Y.; Cheng, Z. J.; Liu, Y. Y. Octopus-inspired smart adhesive with adjustable stiffness for adhesion on uneven surfaces in air and underwater. *Small* **2025**, *21*, e05795.
31 Dai, S. P.; Dong, X.; Jiang, Y. Y.; Ge, J.; Ding, J. N.; Yuan, N. Y. High adhesive force, wide temperature adaptability thermochromic ionogel smart window. *ACS Appl. Polym. Mater.* **2023**, *5*, 3398−3404.
32 Deng, Y. M.; Ni, H. C.; Tang, Y. M.; Liu, B. J.; Ding, H. Y.; Wang, G. P.; Zheng, S. Y.; Yang, J. T. Biomimetic underwater adhesives based on IL-mediated coacervation. *Mater. Horiz.* **2026**, *13*, 840−850.
33 Yao, L.; Huang, Y.; Chen, G. Q.; Zhou, Z. Q.; Zhu, H.; Zhang, Q.; Zhu, S. P. Anti-creep adhesive tapes via trapped-entanglement-regulated topological networks. *Adv. Mater.* **2026**, *38*, e13105.
34 Hu, Y. X.; Liu, K.; Wu, P. Y. Strong underwater supramolecular adhesives via fluorinated ionic liquids. *Adv. Funct. Mater.* **2025**, *35*, 2502134.
35 Wang, B. M.; Qiao, C. Y.; Wang, Y. L.; Dong, X. X.; Zhang, W. Q.; Lu, Y.; Yuan, J. Y.; Zeng, H. B.; Wang, H. Multifunctional underwater adhesive film enabled by a single-component poly(ionic liquid). *ACS Nano* **2023**, *17*, 5871−5879.
36 Li, Y. P.; Jin, Y.; Zeng, W. H.; Jin, H. Y.; Shang, X.; Zhou, R. Bioinspired fast room-temperature self-healing, robust, adhesive, and AIE fluorescent waterborne polyurethane via hierarchical hydrogen bonds and use as a strain sensor. *ACS Appl. Mater. Interfaces* **2023**, *15*, 35469−35482.
37 Bui, K.; Nguyen, G. T. M.; Vancaeyzeele, C.; Vidal, F.; Hu, X.; Wan, C. Y.; Plesse, C. Stretchable, healable, and weldable vitrimer ionogel for ionotronic applications. *Chem. Eng. J.* **2023**, *474*, 145533.
38 Luo, Y. Q.; Zhou, J. Y.; Chen, Y.; Qi, H. S. Multifunctional UV-shielding, fully recyclable, and conductive ionogels with highly adhesion, and superior mechanical performance for smart wearable applications. *Chem. Eng. J.* **2025**, *519*, 165642.
39 Liu, P. M.; Zhang, Y. J.; Yin, D. X.; Chen, J. R.; Guan, R. F.; Cao, D. X.; Gao, Y. J.; Huang, J. Y.; Zhao, S. F. Tough and self-healing solvent-free ionogels enabled by intermolecular mechanical interlocking and multiple dynamic interactions for multifunctional sensing. *Chem. Eng. J.* **2026**, *537*, 176552.
40 Zhang, L. W.; Liu, S.; Wang, Z. Z.; Lei, Z. Y.; Wu, P. Y. An enthalpy-entropy compensated ionogel with a broadband viscoelastic plateau for non-invasive and high-fidelity neurointerfaces. *Adv. Mater.* **2026**, *38*, e21208.
41 Yue, Y. R.; Liang, T. B.; Yao, C. L.; Tang, J. H.; Li, F.; Huo, Y.; Wang, D. C.; Liu, P. J.; Yang, S. J.; Fan, X.; Lin, X. X.; Wang, D.; Sun, K.; Yang, C. D.; Cao, H. J.; Chen, S. S. Directional anchoring doping networks for robust polymeric bioelectronics. *Adv. Mater.* **2026**, *38*, e20074.